Journal of Power Sources 197 (2012) 44–49

Contents lists available at SciVerse ScienceDirect

Journal of Power Sources

journal homepage: www.elsevier.com/locate/jpowsour

Role of Pt-pyridinic nitrogen sites in methanol oxidation on Pt/polypyrrole-carbon black Catalyst

Sheng Zhang*, Hui Wang, Na Zhang, Fandong Kong, Hui Liu, Geping Yin**,[1]

School of Chemical Engineering & Technology, Harbin Institute of Technology, No. 92, West Da-Zhi Street, Harbin 150001 China

ARTICLE INFO

Article history:
Received 9 July 2011
Received in revised form
13 September 2011
Accepted 13 September 2011
Available online 19 September 2011

Keywords:
Pt nanoparticles
Polypyrrole
Tartaric acid
Pt-pyridinic nitrogen sites
Methanol oxidation

ABSTRACT

In the present study, polypyrrole-carbon black (Ppy-C) composite is synthesized via *in situ* chemical polymerization method and then Pt nanoparticles are deposited on the surface of Ppy-C, where tartaric acid is employed as both a reductant and a stabilizer for Pt nanoparticles. Transmission electron microscopy (TEM) and X-ray diffraction (XRD) indicate that Pt nanoparticles have a higher dispersion and smaller particle size (~2.3 nm) on Ppy-C composite than that on carbon black. Electrochemical measurements show that Pt/Ppy-C catalyst Exhibits 60% higher electrocatalytic activity towards methanol oxidation than Pt/C. X-ray photoelectron spectroscopy (XPS) characterization indicates Pt4f binding energy in Pt/Ppy-C is shifted by +0.2 eV as compared with that in Pt/C, while N 1s binding energy in Pt/Ppy-C shifted by −0.5 eV as compared with that in Ppy-C composite. The Pt-pyridinic nitrogen sites suppress the posioning CO adsorption on Pt nanoparticles and facilitate the methanol electrocatalytic oxidation. This work is important for the understanding of the role of Ppy in the fuel cell electrocatalyst, and the development of advanced catalysts for methanol oxidation.

1. Introduction

Low temperature fuel cells are attracting much attention as an alternative to conventional internal combustion engines and secondary batteries [1–4]. Much effort has been devoted to developing low temperature fuel cells in the last few decades, and great advances have been achieved [5]. However, it is still challenging to commercialize them because of the prohibitive cost and poor durability [6–8]. Catalysts play a key role in both the cost and the durability of low temperature fuel cells [9]. The conventional fuel cell electrocatalysts are Pt-based nanoparticles supported on porous conductive supporting materials with a high specific surface area.

The support materials can interplay with Pt nanoparticles, which influences the catalytic activity. The catalyst durability is also greatly dependent on its support. Vulcan XC-72 carbon black [10] and carbon nanotubes (CNT) [11,12] are two most common support materials for electrocatalysts in fuel cells because of the high specific surface area and high electrical conductivity. Novel nanostructured carbon materials such as carbon nanofibers [13], mesoporous carbon [14,15], carbon nanosphere [16], and grapheme [17,18] are also developed as catalyst supports. And due to the high electron transfer rate and high electrochemical stability, carbon materials with ordered graphitic structure can also be used as promising support [19].

Recently, conducting polymers have attracted considerable attentions due to the promising applications in energy storage/conversion, optoeletronics, chemical sensors, and separations [20,21]. Among conducting polymers, polypyrrole (Ppy) has been used as a promising support material due to its high electrical conductivity and facile preparation [22,23]. Ppy can cover pores and other geometrically restricted portions on the surface of carbon support [24]. More importantly, Ppy can influence the catalytic activity of electrocatalysts [25–27]. The composite of Ppy and carbon supports permits a large surface area, high electrical conductivity, and facile flow of electronic charges for the electrochemical processes. Zelenay et al. [28] used simple chemical method to synthesize cobalt-polypyrrole-carbon (Co-Ppy-C) catalysts, where Ppy was solely used as a matrix for entrapping cobalt and generating active Co–N sites for oxygen reduction reaction (ORR). Fuel cell tests showed that the Co-Ppy-C catalysts delivered high ORR activity without any noticeable loss in performance over 100 h operating times. Selvaraj et al. [29] synthesized Ppy-CNT composite by *in situ* polymerization, and then deposited Pt nanoparticles on the Ppy-CNT by an HCHO reduction method. The obtained catalysts showed higher activities towards methanol oxidation than Pt/C catalysts, which was attributed to the increase in electrochemically accessible surface areas due to the combined effect of polymers and carbon nanotubes. Yang et al. [26]

* Corresponding author. Tel.: +86 451 86417853.
** Corresponding author. Tel.: +86 451 86413707.
E-mail addresses: zhangsheng1982@hit.edu.cn (S. Zhang), yingphit@hit.edu.cn (G. Yin).
[1] Tel.: +86 451 86413707.

0378-7753/$ – see front matter © 2011 Elsevier B.V. All rights reserved.
doi:10.1016/j.jpowsour.2011.09.031

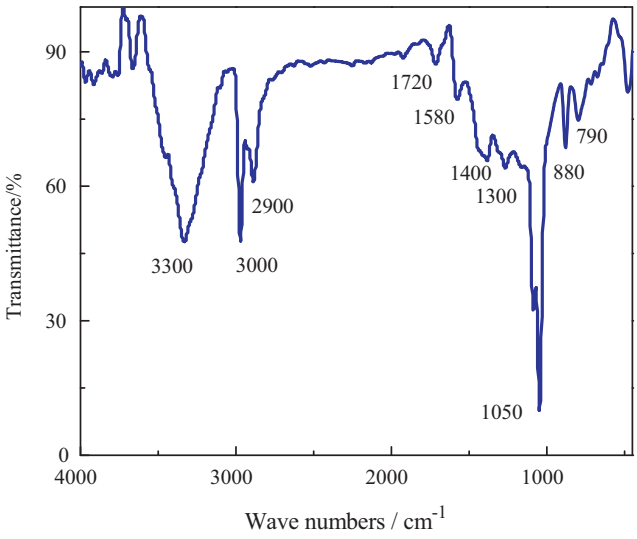

Fig. 1. FT-IR spectrum of Ppy-C composite.

synthesized nanostructured polypyrrole/carbon composite synthesized by *in situ* chemical oxidative polymerization of pyrrole on Vulcan XC-72 carbon. The catalysts exhibited higher methanol oxidation activity and better CO tolerance than conventional Pt/C catalysts, which might be due to the higher electrochemically available surface areas, electronic conductivity, and higher dispersion and utilization of deposited Pt nanoparticles.

However, few reports have studied on the underlying reasons for Ppy improving the eletrocatalytic activity of Pt catalyst. It has been observed that Pt nanoparticles are more homogeneously anchored onto Ppy-C composite support than XC-72 carbon black. Therefore it is expected that a strong interaction exists between Pt nanoparticles and Ppy. However no investigation has been performed on the effect of this interaction on the electrocatalysts' performance. In the present study, the obtained Pt nanoparticles uniformly deposited on the Ppy-C support exhibited higher electrocatalytic activity and durability towards methanol oxidation than Pt/C. And detailed experiments explored the presence of electron transfer between Pt nanoparticles and pyridinic nitrogen sites in Ppy, which resulted in the high electrocatalytic performance of Pt/Ppy-C catalysts.

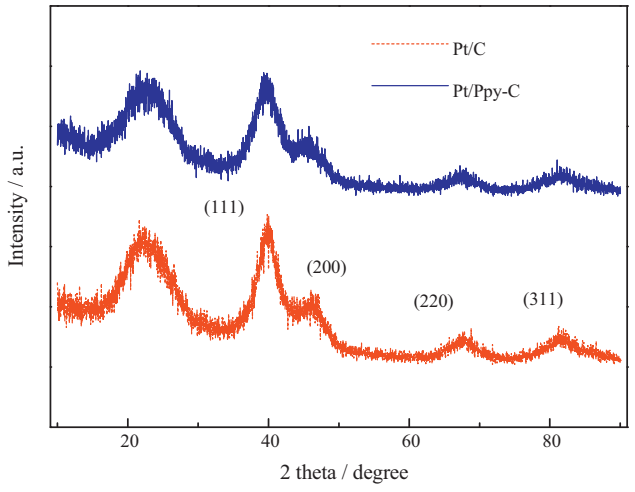

Fig. 2. XRD patterns of Pt/C and Pt/Ppy-C.

2. Experimental methods

2.1. Catalyst preparation

Pyrrole monomer was obtained from Sinopharm Chemical Reagent Co. Ltd. and purified by distillation under the protection of high purity argon. Vulcan XC-72 carbon powder was obtained from Cabot Company and $H_2PtCl_6{\cdot}6H_2O$ was purchased from Aldrich. Tartaric acid was obtained from Beijing Chemical Reagent Company.

Ppy-C composite was synthesized by *in situ* polymerization method. 0.15 g Vulcan XC-72 powder was uniformly dispersed into 150 ml ethanol solution under ultrasonic treatment for 30 min, followed by adding 0.734 mmol $(NH_4)_2S_2O_8$. The obtained mixture was stirred for 1 h. Then a freshly prepared pyrrole solution (25 μl pyrrole monomer solved in 50 ml ultra-pure water) was slowly added to the above suspension solution and kept stirring for 5 h. After reaction, the product was filtered and washed with ultra-pure water and ethanol until the filtrate was colorless. The obtained black power was dried for 5 h at 80 °C in a vacuum condition.

20 mass % Pt/Ppy-C catalyst was prepared by a modified colloidal method [30]. In brief, the catalysts were synthesized as follows. 500 mg tartaric acid and 0.052 mmol H_2PtCl_6 were dissolved in ultra-pure water, and then sodium hydroxide was added to adjust the solution pH value to 10. Meanwhile, 40 mg Ppy-C was dispersed in 50 ml isopropyl alcohol solution followed by ultrasonic treatment for 1 h, and then added to the above H_2PtCl_6 solution and stirred for additional 2 h. Then the suspension solution was heated to 96 °C under reflux for 3 h. During the reaction, a flow of argon gas passed through the reaction system to remove the oxygen. The solution was cooled down to room temperature with continuous stirring, and then 0.1 mol L^{-1} HNO_3 was added into the suspension solution to adjust the solution pH value to 4. The mixture was stirred for 12 h and then filtered and washed with plenty of ultra-pure water, and finally dried at 80 °C for 5 h. As a contrast, Pt/C catalyst was prepared using the same method.

2.2. Materials characterization

Fourier transform infrared (FTIR) analysis was carried out using a NICOLETiS10 spectrometer. The spectra were obtained by mixing the sample with KBr. The X-ray diffraction (XRD) patterns were obtained using the D/max-rB diffractometer (made in Japan) using a Cu Kα X-ray source at 45 kV and 100 mA. The transmission electron microscopy (TEM) images of the catalysts were taken in a microscope equipped with an Oxford ISIS system. X-ray photoelectron spectroscopy (XPS) measurements are made using a Physical Electronics Quantum-5600 Scanning ESCA Microprobe. The Al X-ray source operated at 250 W. The sample to analyzer takeoff angle was 45°. Survey spectra were collected at pass energy (PE) of 187.85 eV over the binding energy range 0–1300 eV. High binding energy resolution Multiplex data for the individual elements were collected at a PE of 29.55 eV.

2.3. Electrochemical measurement

Electrochemical measurements were performed at a standard three-electrode electrochemical cell controlled with a CHI 650d electrochemical working station with Pt foil and Hg/Hg_2SO_4 as the counter electrode and reference electrode, respectively. The catalyst powder was dispersed in the water to obtain a homogeneous black suspension solution (2 mg ml^{-1}). Then 5 μL of this solution was applied onto the surface of a glassy carbon electrode. After the paste was dried in room temperature, a 5 μL of 5 wt% Nafion in ethanol solution spread on the catalyst. The well-prepared

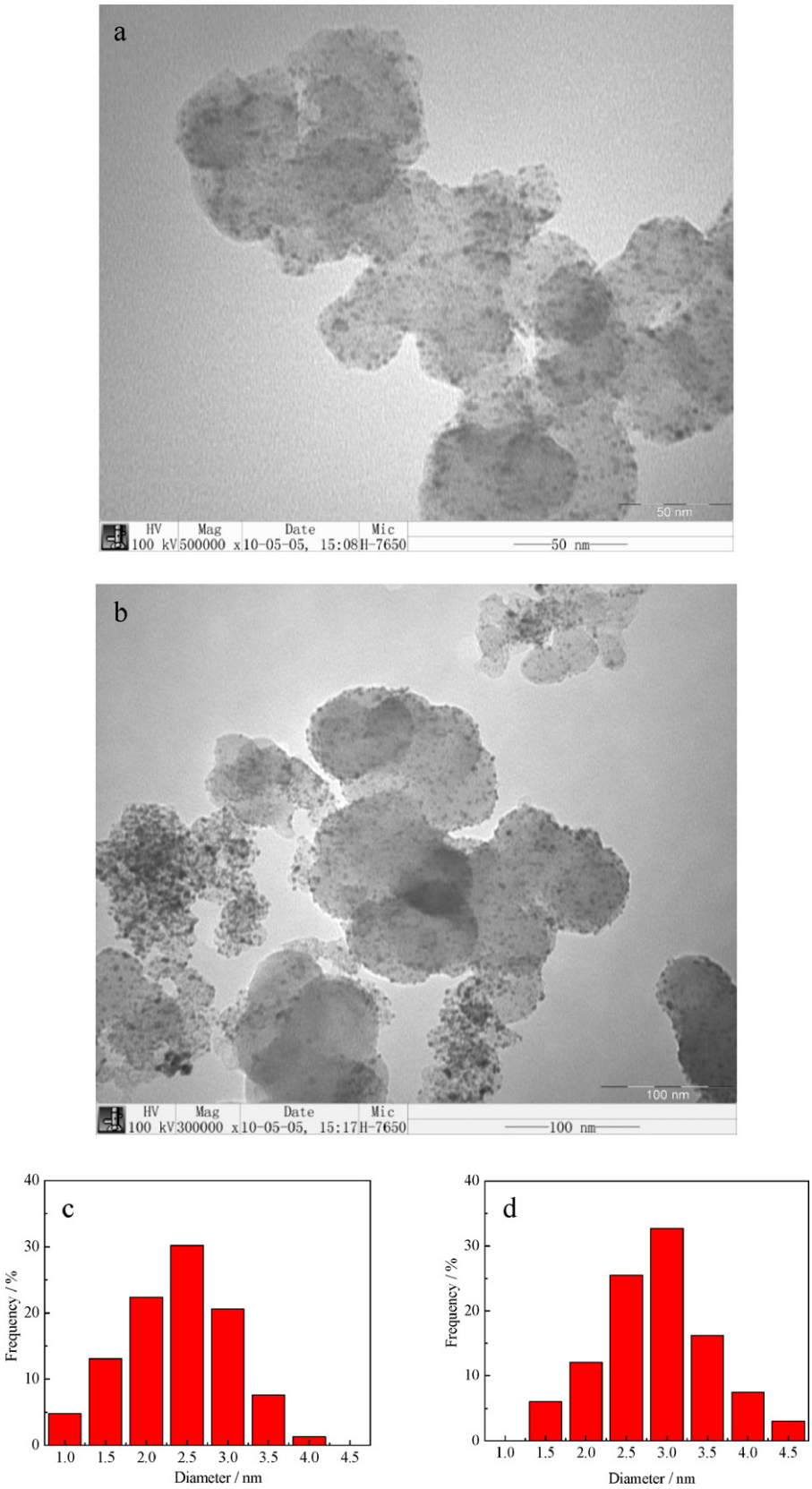

Fig. 3. TEM images and Pt nanoparticles size distribution of Pt/Ppy-C (a and c) and Pt/C (b and d).

electrode was dried overnight at room temperature before electrochemical tests.

The working electrode was first activated using cyclic voltammograms (CVs) (0.5–1.2 V at 50 mV s^{-1}) in Ar-purged 0.5 M H_2SO_4 solution until a steady CV curve was obtained. Electrochemical oxidation of methanol on the Pt/C is carried out in 0.5 M CH_3OH + 0.5 M H_2SO_4 solutions by the CV technique at 50 mV s^{-1} between 0.05 and 1.2 V. The amperometric current density–time (i–t) curves were measured for 1 h at a fixed potential of 0.6 V. For the CO stripping experiments, CO was absorbed by holding the electrode at 0.08 V in CO saturated 0.5 M H_2SO_4 for 20 min, followed by removal of CO in the solution by purging argon for 20 min while still holding the electrode potential at 0.08 V. Then CO stripping voltammograms were performed at a scan rate of 20 mV s^{-1}.

All potentials in these studies are reported versus RHE. All the electrochemical experiments are carried out at 25 °C.

3. Result and discussion

3.1. Materials characterization

In the present work, Ppy-C composite is synthesized by *in situ* chemical polymerization method. FTIR of obtained Ppy-C is shown in Fig. 1, which was similar to chemical synthesized pure Ppy [31]. All feature peaks of Ppy can be observed in Fig. 1. The broad peak at approximately 3300 cm^{-1} is the typical N–H stretch. The characteristic peaks at 1580 cm^{-1} and 1400 cm^{-1} can be assigned to the C=C stretching, whereas the peak at 1720 cm^{-1} represents to C=N bond [31]. Two peaks observed at around 1300 cm^{-1} and 1050 cm^{-1} are attributed to the plane vibration and breathing of pyrrole rings, respectively [32]. The peaks at 880 cm^{-1}, 790 cm^{-1} are attributed to C–H wagging [33]. Therefore, the peaks observed in our present work match well with the ones available in the literature, which confirms the formation of Ppy.

XRD patterns of Pt/C and Pt/Ppy-C catalysts are shown in Fig. 2. The diffraction peaks at the Bragg angles of 39.7°, 46.2°, 67.4°, and 81.2° are respectively ascribed to Pt(1 1 1), Pt(2 0 0), Pt(2 2 0), and Pt(3 1 1) characteristic diffraction, indicating that Pt nanoparticles in both Pt/C and Pt/Ppy-C catalysts have a face-centered cubic (fcc) structure. The average Pt particle sizes of two catalysts are calculated using the Debye–Scherrer formula [34]:

$$L = \frac{0.9\lambda_{K\alpha 1}}{B_{2\theta}\cos\theta_{max}}$$

where L is the mean size of particles, $\lambda_{K\alpha 1}$ is the X-ray wavelength (λ = 1.5418 Å), θ_{max} is the angle of (2 2 0) peak, and $B_{2\theta}$ is the half-peak width for Pt(2 2 0). The average sizes of Pt nanoparticles are calculated to be 2.7 nm for Pt/C and 2.3 nm for Pt/Ppy-C, respectively, which indicates that Pt nanoparticles in Pt/Ppy-C have smaller size than that in Pt/C.

Fig. 3 shows TEM images and Pt nanoparticle size distributions of Pt/Ppy-C and Pt/C catalysts, where Pt nanoparticles on the surface of Ppy-C demonstrate higher dispersion than that on the conventional XC-72 carbon black. The Pt nanoparticles highly dispersed on Ppy-C composites provides a favorable condition for good electrochemical performance. The average sizes of the Pt nanoparticles in Pt/Ppy-C and Pt/C catalysts are 2.4 nm and 2.7 nm, respectively, which is consistent with the results calculated from XRD patterns. The *in situ* polymerization of Ppy made XC-72 carbon black "smooth" and promoted Pt nanoparticles to disperse uniformly on the Ppy-C composite with improved adhesion [24]. And the small diameter and high dispersion of Pt nanoparticles on the surface of Ppy-C support can be attributed to the fact that the nitrogen sites in Ppy might provide main initial nucleation sites for the formation of Pt nanoparticles [35].

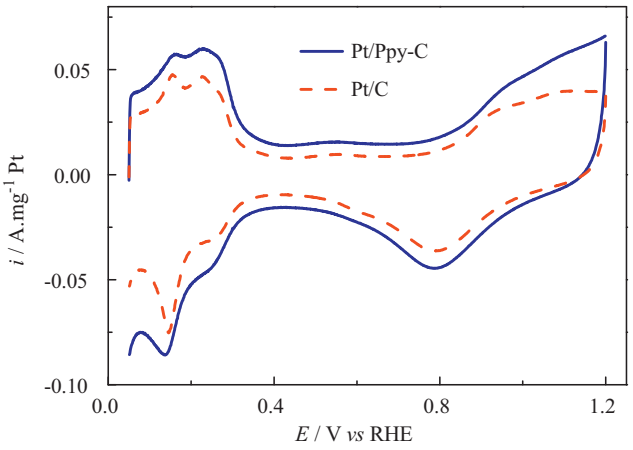

Fig. 4. Cyclic voltammograms of Pt/C and Pt/Ppy-C in Ar-saturated 0.5 mol L^{-1} H_2SO_4 solution.

In the synthesis of Pt nanoparticles, tartaric acid acted as not only a reductant, but also a stabilizer [36]. Tartaric acid is a weak reductant. No variation in the color of a mixture of tartaric acid and H_2PtCl_6 was observed under room temperature. Therefore, the reduction reaction of H_2PtCl_6 by tartaric acid was required at higher temperature (96 °C). Like sodium citrate, the carboxyl groups of tartaric acid can absorb on the surface of Pt nanoparticles, and generate an electrostatic double layer around nanoparticles which prevent nanoparticles from aggregation [37]. The electrostatic double layer is very sensitive to the environment, so the adjustment of pH can impair electrostatic repulsion between nanoparticles and promote Pt nanoparticles to load on the carbon supporting materials (XC-72 and Ppy-C).

3.2. Electrochemical properties

Fig. 4 shows the cyclic voltammograms (CVs) of Pt/Ppy-C and Pt/C performed in 0.5 M H_2SO_4 solution at a sweep rate of 50 mV s^{-1}. Typical hydrogen and oxygen adsorption/desorption behavior can be clearly observed on both Pt/C and Pt/Ppy-C catalysts. The electrochemical surface area (ESA) of Pt can be calculated with coulombic charges accumulated during hydrogen adsorption and desorption:

$$\mathrm{ESA} = \frac{Q_H}{0.21 \times [\mathrm{Pt}]}$$

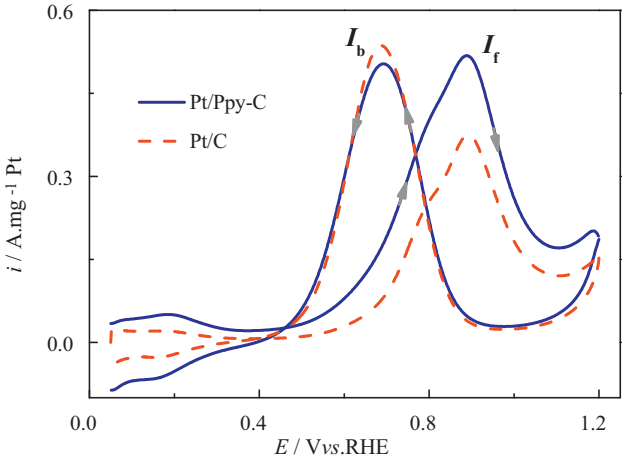

Fig. 5. CH_3OH oxidation activity on Pt/C and Pt/Ppy-C in 0.5 M CH_3OH and 0.5 M H_2SO_4.

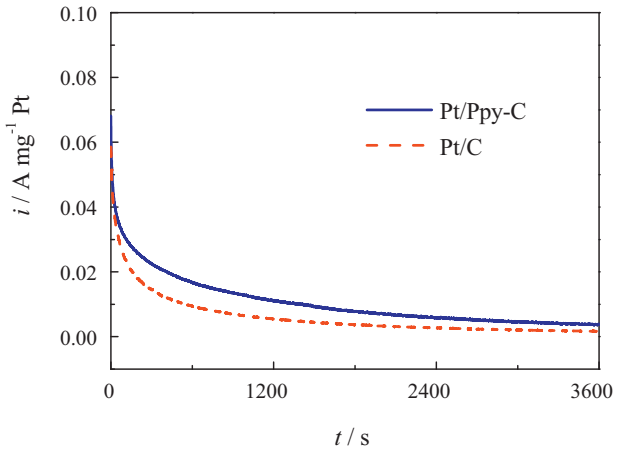

Fig. 6. Amperometric *i–t* curves of CH_3OH electro-oxidation on Pt/Ppy-C and Pt/C catalysts in N_2-saturated 0.5 M CH_3OH and 0.5 M H_2SO4 at a fixed potential of 0.6 V.

where Q_H (mC) is the charge due to the hydrogen adsorption/desorption in the hydrogen region (0.05–0.4 V) of the CVs, 0.21 mC cm^{-2} is the electrical charge associated with monolayer adsorption of hydrogen on Pt, and [Pt] is the loading of Pt on the working electrode. Results show that ESAs of Pt/C and Pt/Ppy-C are 54.5 m^2 g^{-1} Pt and 60.9 m^2 g^{-1} Pt respectively. The higher ESA of Pt/Ppy-C electrocatalyst can be attributed to the uniform distribution and small particle size of Pt nanoparticles.

The electrocatalytic activity towards methanol oxidation on Pt/C and Pt/Ppy-C catalysts are investigated. Fig. 5 clearly shows an oxidation peak around 0.88 V in the anodic scan region, which can be ascribed to the oxidation of methanol adsorbed on Pt surface [38,39]. In the forward scan, the peak current density (I_p) of Pt/Ppy-C (0.55 A·mg^{-1} Pt) is 60% higher than that of Pt/C (0.34 A mg^{-1} Pt). And the specific current density of Pt/Ppy-C is 9.0 A m^{-2} Pt, much higher than that of Pt/C (6.2 A m^{-2} Pt), indicating a much better methanol oxidation activity on Pt/Ppy-C electrocatalyst. Fig. 6 shows the amperometric *i–t* curves on Pt/Ppy-C and Pt/C electrocatalysts in the solution of 0.5 M CH_3OH + 0.5 M H_2SO_4 at a fixed potential of 0.6 V. The current density at 3600s on the Pt/Ppy-C catalyst is 0.004 A mg^{-1} Pt, which is about two times that on the Pt/C catalyst (0.002 A mg^{-1} Pt). And the corresponding specific current density is 0.067 A m^{-2} Pt, much higher than that of Pt/C (0.037 A m^{-2} Pt). This demonstrates that the electrocatalytic durability of the Pt/Ppy-C catalyst towards methanol oxidation is much higher than that of the Pt/C catalyst [40].

To elucidate the underlying reasons for the improvement in the catalytic activity towards methanol oxidation, we employed XPS to characterize the Pt/Ppy-C and Pt/C catalysts. Fig. 7a shows the survey XPS spectra of Ppy-C, Pt/Ppy-C, and Pt/C, where the elements of Pt, C, O, and N are observed on these samples. According to the XPS results, the N content of Pt/Ppy-C is 5.98 at %, which confirm the presence of Ppy in the catalyst. Pt 4f XPS spectra peak of Pt/Ppy-C in Fig. 7b exhibits doublet peaks at 71.8 and 75.0 eV, which can be attributed to Pt^0 $4f_{7/2}$ and Pt^0 $4f_{5/2}$, respectively, indicating that Pt nanoparticles exist in metallic form [41]. And Fig. 7b also indicated that Pt4f binding energy of Pt nanoparticles in Pt/Ppy-C shifted by +0.2 eV as compared with that in Pt/C. Meanwhile, Fig. 7c indicated that N 1s binding energy in Pt/Ppy-C shifted by −0.5 eV as compared with that in Ppy-C composite. If we consider that the reference level (C 1s, set to 284.5 eV for calibration) has no change in the measurement, the change of the binding energy of Pt 4f and

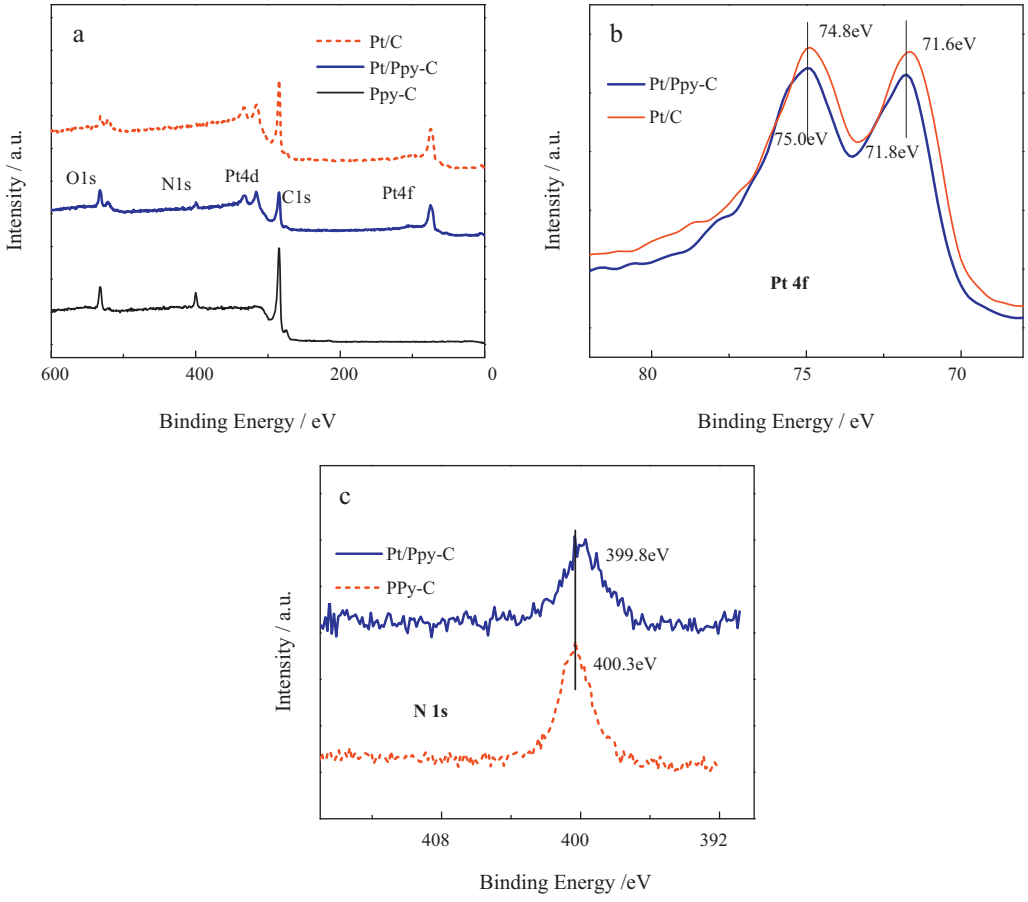

Fig. 7. Survey XPS spectra (a) of Ppy-C, Pt/Ppy-C, and Pt/C; N 1s XPS spectra (b) of Ppy-C and Pt/Ppy-C; Pt 4f XPS spectra of Pt/C and Pt/Ppy-C (c).

N 1s is most likely due to the electron transfer between Pt and N in Pt/Ppy-C catalyst [34,42,43], which indicates the strong Pt–N interaction in Pt/Ppy-C. It has been reported that the nitrogen functional groups on support surface can intensify the electron withdrawing effect against Pt and the decreased electron density of platinum (consistent with the XPS results above), facilitates the methanol electrocatalytic oxidation and oxygen reduction reaction [44,45]. Watanabe et al. reported that PtCo alloy showed higher Pt4f BE value than pure Pt, and the former exhibited higher methanol oxidation activity [46,47]. Therefore, the strong electronic interaction between Pt nanoparticles and pyridinic nitrogen sites in Pt/Ppy-C catalyst can explain why the Pt/Ppy-C catalyst showed higher catalytic activity towards methanol oxidation than Pt/C catalyst. Meanwhile, the interaction between Pt nanoparticles and pyridinic nitrogen sites can also keep Pt nanoparticles firmly bounded to the support and prevent Pt nanoparticles from aggregating and detaching from the surface of Ppy-C support [48].

4. Conclusions

In this report, Pt/Ppy-C catalyst was synthesized and exhibited high electrocatalytic activity towards methanol oxidation. Pt nanoparticles had a higher dispersion and smaller particle size on Ppy-C composite than that on carbon black, which can be attributed to the fact that the pyridinic nitrogen sites in Ppy might provide the main initial nucleation sites for the formation of Pt nanoparticles. More importantly, Pt/Ppy-C catalyst exhibited much higher electrocatalytic activity and durability towards methanol oxidation than Pt/C catalyst. The Pt-pyridinic nitrogen sites in Pt/Ppy-C catalyst suppress the posioning CO adsorption on Pt nanoparticles and facilitate the methanol electrocatalytic oxidation. Thus, the present study reveals the importance of Pt-pyridinic nitrogen sites for enhancing catalytic activity and durability of fuel cell electrocatalyst.

Acknowledgements

This work is financially supported by National Natural Science Foundation of China (Grant No. 50872027, 21106024, and 21173062), Natural Scientific Research Innovation Foundation in Harbin Institute of Technology (XWQQ5750012411), and Fundamental Research Funds for the Central Universities (HIT.ICRST.2010006).

References

[1] Y. Wang, C.Y. Wang, J. Electrochem. Soc. 154 (2007) B636–B643.
[2] S.Y. Huang, P. Ganesan, S. Park, B.N. Popov, J. Am. Chem. Soc. 131 (2009) 13898–13899.
[3] C.Y. Du, T.S. Zhao, Z.X. Liang, J. Power Sources 176 (2008) 9–15.
[4] S. Zhang, Y.Y. Shao, G.P. Yin, Y.H. Lin, Angew. Chem. Int. Ed. 49 (2010) 2211–2214.
[5] J.J. Wang, Y.G. Chen, H. Liu, R.Y. Li, X.L. Sun, Electrochem. Commun. 12 (2010) 219–222.
[6] X.W. Yu, S.Y. Ye, J. Power Sources 172 (2007) 145–154.
[7] J. Zhang, K. Sasaki, E. Sutter, R.R. Adzic, Science 315 (2007) 220–222.
[8] Y.Y. Shao, S. Zhang, C.M. Wang, Z.M. Nie, J. Liu, Y. Wang, Y.H. Lin, J. Power Sources 195 (2010) 4600–4605.
[9] S. Wang, S.P. Jiang, T.J. White, J. Guo, X. Wang, J. Phys. Chem. C 113 (2009) 18935–18945.
[10] J. Ge, W. Xing, X. Xue, C. Liu, T. Lu, J. Liao, J. Phys. Chem. C 111 (2007) 17305–17310.
[11] S. Zhang, Y.Y. Shao, G.P. Yin, Y.H. Lin, J. Mater. Chem. 20 (2010) 2826–2830.
[12] K.P. Gong, F. Du, Z.H. Xia, M. Durstock, L.M. Dai, Science 323 (2009) 760–764.
[13] E.S. Steigerwalt, G.A. Deluga, D.E. Cliffel, C.M. Lukehart, J. Phys. Chem. B 105 (2001) 8097–8101.
[14] Z.H. Wen, J. Liu, J.H. Li, Adv. Mater. 20 (2008) 743–747.
[15] Y.Y. Shao, S. Zhang, R. Kou, X.Q. Wang, C.M. Wang, S. Dai, V. Viswanathan, J. Liu, Y. Wang, Y.H. Lin, J. Power Sources 195 (2010) 1805–1811.
[16] S. Sun, F. Jaouen, J.-P. Dodelet, Adv. Mater. 20 (2008) 3900–3904.
[17] S. Zhang, Y. Shao, H.-G. Liao, J. Liu, I.A. Aksay, G. Yin, Y. Lin, Chem. Mater. 23 (2011) 1079–1081.
[18] R. Kou, Y.Y. Shao, D.H. Wang, M.H. Engelhard, J.H. Kwak, J. Wang, V.V. Viswanathan, C.M. Wang, Y.H. Lin, Y. Wang, I.A. Aksay, J. Liu, Electrochem. Commun. 11 (2009) 954–957.
[19] P.V. Shanahan, L. Xu, C. Liang, M. Waje, S. Dai, Y.S. Yan, J. Power Sources 185 (2008) 423–427.
[20] J.C. Wu, W.M. Mullett, J. Pawliszyn, Anal. Chem. 74 (2002) 4855–4859.
[21] J. Wang, S. Chan, R.R. Carlson, Y. Luo, G.L. Ge, R.S. Ries, J.R. Heath, H.R. Tseng, Nano Lett. 4 (2004) 1693–1697.
[22] T.S. Olson, S. Pylypenko, P. Atanassov, K. Asazawa, K. Yamada, H. Tanaka, J. Phys. Chem. C 114 (2010) 5049–5059.
[23] Y. Yuan, S.G. Zhou, L. Zhuang, J. Power Sources 195 (2010) 3490–3493.
[24] S.M. Unni, V.M. Dhavale, V.K. Pillai, S. Kurungot, J. Phys. Chem. C 114 (2010) 14654–14661.
[25] V. Selvaraj, M. Alagar, I. Hamerton, J. Power Sources 160 (2006) 940–948.
[26] H.B. Zhao, L. Li, J. Yang, Y.M. Zhang, J. Power Sources 184 (2008) 375–380.
[27] J.W. Liu, J.X. Qiu, Y.Q. Miao, J.R. Chen, J. Mater. Sci. 43 (2008) 6285–6288.
[28] R. Bashyam, P. Zelenay, Nature 443 (2006) 63–66.
[29] V. Selvaraj, M. Alagar, Electrochem. Commun. 9 (2007) 1145–1153.
[30] S. Zhang, Y.Y. Shao, G.P. Yin, Y.H. Lin, J. Power Sources 195 (2010) 1103–1106.
[31] K. Arora, A. Chaubey, R. Singhal, R.P. Singh, M.K. Pandey, S.B. Samanta, B.D. Malhotra, S. Chand, Biosens. Bioelectron. 21 (2006) 1777–1783.
[32] P. Yang, J. Zhang, Y. Guo, Appl. Surf. Sci. 255 (2009) 6924–6929.
[33] B. Tian, G. Zerbi, J. Chem. Phys. 92 (1990) 3886–3891.
[34] S. Zhang, Y.Y. Shao, G.P. Yin, Y.H. Lin, J. Mater. Chem. 19 (2009) 7995–8001.
[35] K. Jiang, A. Eitan, L.S. Schadler, P.M. Ajayan, R.W. Siegel, N. Grobert, M. Mayne, M. Reyes-Reyes, H. Terrones, M. Terrones, Nano Lett. 3 (2003) 275–277.
[36] Y.W. Tan, X.H. Dai, Y.F. Li, D.B. Zhu, J. Mater. Chem. 13 (2003) 1069–1075.
[37] S. Zhang, Y.Y. Shao, X.H. Li, Z.M. Nie, Y. Wang, J. Liu, G.P. Yin, Y.H. Lin, J. Power Sources 195 (2010) 457–460.
[38] Y. Lin, X. Cui, C. Yen, C.M. Wai, J. Phys. Chem. B 109 (2005) 14410–14415.
[39] Z. Liu, X.Y. Ling, X. Su, J.Y. Lee, J. Phys. Chem. B 108 (2004) 8234–8240.
[40] S. Zhang, Y. Shao, H. Liao, M.H. Engelhard, G. Yin, Y. Lin, ACS Nano 5 (2011) 1785–1791.
[41] M. Okamoto, T. Fujigaya, N. Nakashima, Small 5 (2009) 735–740.
[42] H. Tsunoyama, N. Ichikuni, H. Sakurai, T. Tsukuda, J. Am. Chem. Soc. 131 (2009) 7086–7093.
[43] C. Wang, H. Daimon, S. Sun, Nano Lett. 9 (2009) 1493–1496.
[44] T. Maiyalagan, B. Viswanathan, U.V. Varadaraju, Electrochem. Commun. 7 (2005) 905–912.
[45] S.C. Roy, A.W. Harding, A.E. Russell, K.M. Thomas, J. Electrochem. Soc. 144 (1997) 2323–2328.
[46] M. Wakisaka, S. Mitsui, Y. Hirose, K. Kawashima, H. Uchida, M. Watanabe, J. Phys. Chem. B 110 (2006) 23489–23496.
[47] Q. Huang, H. Yang, Y. Tang, T. Lu, D.L. Akins, Electrochem. Commun. 8 (2006) 1220–1224.
[48] Y.Y. Shao, J.H. Sui, G.P. Yin, Y.Z. Gao, Appl. Catal. B: Environ. 79 (2008) 89–99.